Journal of Solid State Chemistry 182 (2009) 327–330

Contents lists available at ScienceDirect

Journal of Solid State Chemistry

journal homepage: www.elsevier.com/locate/jssc

Structural and physical properties of 1:2 *B*-site-ordered perovskite $Ba_3CaIr_2O_9$

J.G. Zhao, L.X. Yang, Y. Yu, F.Y. Li, R.C. Yu, C.Q. Jin *

Beijing National Lab for Condensed Matter Physics, Institute of Physics, Chinese Academy of Sciences, Beijing 100190, PR China

ARTICLE INFO

Article history:
Received 3 August 2008
Received in revised form
13 October 2008
Accepted 22 October 2008
Available online 12 November 2008

Keywords:
Barium iridates
1:2 *B*-site-ordered perovskite
High-pressure sintering
Rietveld analysis
Electrical conductivity
Magnetic susceptibility

ABSTRACT

The high-pressure phase of iridium-based compound $Ba_3CaIr_2O_9$ was synthesized using high-pressure sintering. Being different from the distorted hexagonal $BaTiO_3$ structure of the ambient $Ba_3CaIr_2O_9$, the high-pressure phase crystals into the 1:2 *B*-site-ordered perovskite structure with the space group *P*-3*m*1 ($Z=1$). Through fitting the X-ray powder diffraction (XRD) data with Rietveld analysis, in which the obtained R_p, R_{wp}, and R_{exp} factors are 7.49%, 11.4%, and 4.82%, respectively, the lattice parameters are $a=5.8296(1)$ Å and $c=7.1659(2)$ Å. The atomic coordinates and the main interatomic distances and bond angles were also obtained. The relationship of electrical resistivity versus temperature shows that the high-pressure phase of $Ba_3CaIr_2O_9$ is a semiconductor in the temperature range of 5–300 K. The measurement of temperature dependence of magnetic susceptibility indicates that it is paramagnetic.

1. Introduction

In the alkaline earth oxide iridate $AIrO_3$ ($A=$ Ca, Sr, and Ba), $BaIrO_3$ adopts the distorted 9R $BaRuO_3$ structure at ambient condition, so it is denoted by "9R", with the space group *C*2/*m* [1]. It is the first known ferromagnet that contains a 5*d* transition metal cation in a ternary oxide, with the Curie temperature T_c about 183 K [2]. By treating the "9R" $BaIrO_3$ at 5 GPa and 1000 °C, we obtained the "6H" $BaIrO_3$ [3]. It is a paramagnetic metal. The "6H" or 6H $Ba_3MIr_2O_9$ ($M=$ alkali metals, alkaline earth elements, 3*d* transition metals, and lanthanides) could be easily obtained at ambient pressure (AP) with chemical substitution of 1/3*M* cations for Ir ion in $BaIrO_3$, in which the *M* and Ir ions occupy the corner-shared octahedral sites (in the MO_6 octahedron) and the face-shared octahedral sites (in the Ir_2O_9 dioctahedron), respectively [4–6].

As one of the substitution compounds in *B*-site of $BaIrO_3$, $Ba_3CaIr_2O_9$ adopts the "6H" structure at AP [6]. Rijssenbeek et al. [7] reported that $Ba_3CaRu_2O_9$ transforms to the 1:2 *B*-site-ordered perovskite-type structure at 8 GPa and 1000 °C, with the space group *P*-3*m*1, from the ambient 6H form. The ordered structure is due to the charge and ion radius differences between Ru and Ca cations [8]. As the corresponding iridates with $Ba_3CaRu_2O_9$, the "6H" $Ba_3CaIr_2O_9$ may also transform to the 1:2 *B*-site-ordered perovskite-type structure by high-pressure (HP) sintering. We performed the HP and high-temperature experiments on the "6H" $Ba_3CaIr_2O_9$, and obtained the HP phase of 1:2 *B*-site-ordered perovskite. It crystallizes into the same structure with that of the HP phase of $Ba_3CaRu_2O_9$, which is identified by the X-ray diffraction (XRD) pattern. In this paper, we denoted the two phases of $Ba_3CaIr_2O_9$ produced at different pressures to AP and HP phases, respectively. Fig. 1(a) and (b) shows the schematic views of the two crystallographic forms of $Ba_3CaIr_2O_9$, respectively. Fig. 1(c) shows the structure of the HP-$Ba_3CaIr_2O_9$ viewed along one of the pseudocubic directions of perovskite. For the first time, the structural detail of the HP-$Ba_3CaIr_2O_9$ was obtained based on Rietveld refinement, together with the characterization of its electrical and magnetic properties. The results were also compared in the context of AP-$Ba_3CaIr_2O_9$.

2. Experimental

2.1. Sample synthesis

The AP-$Ba_3CaIr_2O_9$ was synthesized by using the conventional solid-state chemical reaction method. The starting materials were barium carbonate, calcium carbonate and iridium metal of 99.9% purity. Stoichiometric quantities of materials were mixed together, ground about 30 min in an agate mortar, and placed into an Al_2O_3 crucible. Then the powder was calcined for about 12 h at 900 °C in air. The calcined powder was reground, pressed into a pellet at the pressure of 10 MPa, and sintered at 1100 °C for about 72 h in air with two intermediate re-grindings.

A conventional cubic-anvil type HP facility was used to perform the HP sintering experiment. The AP-$Ba_3CaIr_2O_9$ material was pressed into a pellet of 5.0 mm diameter, and then wrapped with gold foil to avoid contamination. The pellet was put into an h-BN sleeve which was in turn inserted into a graphite tube heater. Pyrophyllite was used as the pressure-transmitting

* Corresponding author. Fax: +86 10 82640223.
E-mail address: zhaojinggeng@163.com (C.Q. Jin).

0022-4596/$ - see front matter © 2008 Elsevier Inc. All rights reserved.
doi:10.1016/j.jssc.2008.10.034

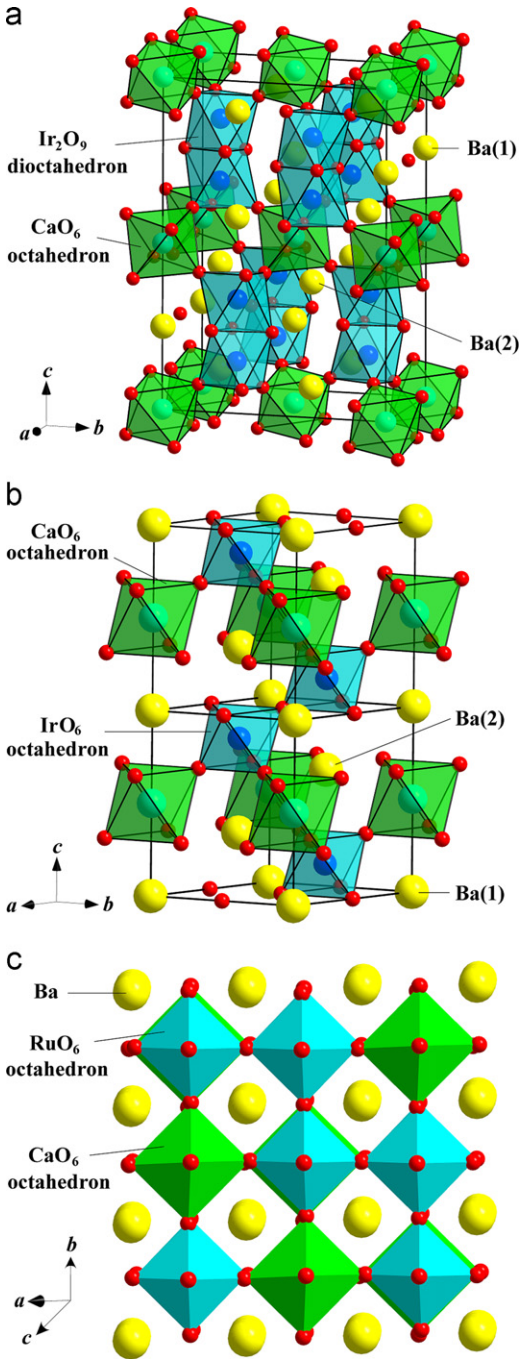

Fig. 1. Schematic views of the (a) AP- and (b) HP-$Ba_3CaIr_2O_9$. The unit cells are outlined. The IrO_6 and CaO_6 octahedrons are represented by geometrical figures (Ir and Ca at the center, O at the corners). (c) Structure of the HP-$Ba_3CaIr_2O_9$ viewed along one of the pseudocubic directions of perovskite.

medium. The treating process was carried out at 5.0 GPa and 1000 °C for about 30 min, followed by a quench from high temperature before pressure release with the rate about 0.6 GPa/min. The product was the HP-$Ba_3CaIr_2O_9$.

2.2. XRD analysis

The structures of our samples were checked by the powder XRD with Cu-$K\alpha$ radiation at room temperature, using a Rigaku diffractometer (MXP-AHP18). The experimental data were collected in 2θ-steps of 0.02° and 3 s counting time in the range of 10–120° and analyzed with Rietveld method by using the FullProf program [9].

2.3. Electrical resistivity measurements

The measurements of temperature dependence of electrical resistivity were performed using the four-probe method with Ag paste contacts on an Oxford Maglab measuring system in the temperature range of 5–300 K.

2.4. Magnetic susceptibility measurements

The relationships of magnetic susceptibility versus temperature were obtained by using a SQUID magnetometer (Quantum Design, MPMS-5S) in the temperature range of 5–300 K. Data were collected under both zero-field-cooled (ZFC) and field-cooled (FC) conditions in an applied field of 1 T. The magnetic field dependence of magnetization for the HP-$Ba_3CaIr_2O_9$ was measured at 5 K with $0\,T \leqslant H \leqslant 5\,T$.

3. Results and discussion

3.1. Crystal structure

Fig. 2 shows the observed and fitted XRD patterns of the HP-$Ba_3CaIr_2O_9$. The data are fitted with the *P*-3*m*1 space group and analyzed with the Rietveld method. The obtained R_p, R_{wp}, and R_{exp} factors are 7.49%, 11.4%, and 4.82%, respectively, indicating the good consistence of the refined results. Although we did not know what the impurity is, we can confirm that it is not the ferromagnetic iridate oxide that includes the "9R" $BaIrO_3$, Sr_2IrO_4 and $Sr_3Ir_2O_7$ [10–12]. The effect of impurity on the physical properties is very small, due to the little content in the whole sample. The lattice parameters are refined to be $a = 5.8296(1)$ Å and $c = 7.1659(2)$ Å, respectively, and the unit cell volume is $210.89(1)$ Å^3. We also refined the XRD data of the AP-$Ba_3CaIr_2O_9$ with the Rietveld method based on the *C*2/*c* space group. The lattice parameters are $a = 5.9136(3)$ Å, $b = 10.2277(5)$ Å, $c = 14.7551(6)$ Å, and $\beta = 91.120(3)°$, and the unit cell volume is $892.26(7)$ Å^3, which are close to those in [6]. So the shrinkage of volume of the HP-$Ba_3CaIr_2O_9$ is about 5.5%, compared with the ambient phase. Tables 1 and 2 list the positional parameters and the main interatomic distances and bond angles for the

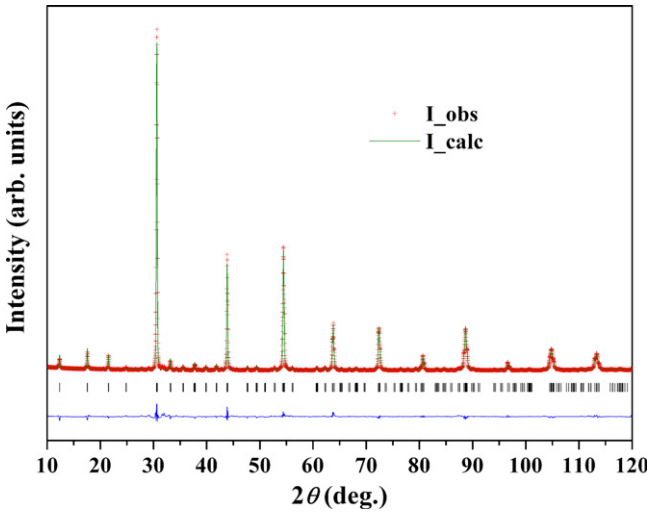

Fig. 2. Experimental (open circle) and fitted (line) X-ray diffraction patterns for the HP-$Ba_3CaIr_2O_9$. The difference plot is shown at the bottom.

Table 1
Atomic coordinates for the HP-$Ba_3CaIr_2O_9$.

Atom	Site	x	y	z	B (Å^2)
Ba(1)	1a	0	0	0	0.88 (6)
Ba(2)	2d	1/3	2/3	0.6659 (4)	0.48 (5)
Ca	1b	0	0	0.5	2.1 (2)
Ir	2d	1/3	2/3	0.1623 (3)	0.51 (4)
O(1)	3e	0.5	0	0	1.6 (3)
O(2)	6i	0.179 (1)	0.821 (1)	0.324 (1)	1.8 (2)

Table 2
Selected bond distances (Å) and angles (deg) for the HP-$Ba_3CaIr_2O_9$.

Bond	Distance (Å)	Bond	Angle (deg)
Ba(1)–O(1) × 6	2.915 (1)	O(1)–Ir–O(1) × 3	90.9 (1)
Ba(1)–O(2) × 6	2.942 (6)	O(1)–Ir–O(2) × 6	90.5 (2)
Ba(2)–O(1) × 6	2.926 (2)	O(1)–Ir–O(2) × 3	178.0 (2)
Ba(2)–O(2) × 6	2.918 (6)	O(2)–Ir–O(2) × 3	88.0 (3)
Ca–O(2) × 6	2.204 (7)	O(2)–Ca–O(2) × 6	89.5 (2)
Ir–O(1) × 3	2.046 (1)	O(2)–Ca–O(2) × 6	90.5 (2)
Ir–O(2) × 3	1.942 (6)	O(2)–Ca–O(2) × 3	180.0 (2)
Ir–Ir	4.091 (2)	Ir–O(1)–Ir	180.0 (1)
Ir–Ca	4.145 (1)	Ir–O(2)–Ca	178.3 (3)

HP-$Ba_3CaIr_2O_9$, respectively. The average Ir–O and Ca–O distances are 1.994(4) and 2.204(7) Å, respectively. For the AP-$Ba_3CaIr_2O_9$, the corresponding distances are 1.998(9) and 2.220(13) Å, respectively. Compared with the ambient phase, the HP-$Ba_3CaIr_2O_9$ has the smaller Ir–O and Ca–O distances.

The ambient $Ba_3MRu_2O_9$ ($M = 3d$ transition metals) cannot transform to 1:2 *B*-site-ordered perovskite structures under HP, due to the approximate ion radius between Ru and *M* cations [8]. Although $Ba_3LnRu_2O_9$ (Ln = lanthanides) compounds adopt the 6H structure at AP, they cannot become perovskite structure under HP, because the Ba_2LnRuO_6 of 1:1 *B*-site-ordered perovskite structure can be synthesized more easily, even at AP [13,14]. So $Ba_3LnRu_2O_9$ is an equimolar mixture of Ba_2LnRuO_6 and 6H $BaRuO_3$ under HP and high temperature [7]. The AP-$Ba_3CaRu_2O_9$ does not decompose under high temperature and HP, because it is difficult to synthesize Ba_2CaRuO_6 at ambient condition, due to the large difference in ion radius between Ca^{2+} and Ru^{6+} cations [8]. Ba_2CaIrO_6 was only synthesized under high O_2 pressure [15], so the AP-$Ba_3CaIr_2O_9$ does not decompose into Ba_2CaIrO_6 and $BaIrO_3$ under high temperature and HP. Therefore, we can obtain the 1:2 *B*-site-ordered perovskite $Ba_3CaIr_2O_9$ by HP sintering.

3.2. Electrical properties

The temperature dependences of electrical resistivity of the AP- and HP-$Ba_3CaIr_2O_9$ are shown in Fig. 3. The AP-$Ba_3CaIr_2O_9$ is a semiconductor. When the AP-$Ba_3CaIr_2O_9$ transforms to the HP form, the electrical resistivity drops about three orders of magnitude at 300 K, and is much smaller than that of most typical semiconductors. In the AP-$Ba_3CaIr_2O_9$, the Ir cations between the two neighbor Ir_2O_9 dioctahedra are separated by Ca cations. So the Ir–Ir dimers are isolated from each other. However, in the HP-$Ba_3CaIr_2O_9$, the Ir cations between the two neighbor IrO_6 octahedra connect to each other through the O anions in the corner, and there is the exchange interaction between them. The IrO_6 octahedra constitute a two-dimensional plane, which is separated by the CaO_6 octahedra plane. So the electrical resistivity of the HP-$Ba_3CaIr_2O_9$ is much smaller than that of the ambient phase. But the HP-$Ba_3CaIr_2O_9$ is not still metallic, due to the energy of the vacant Ca orbitals.

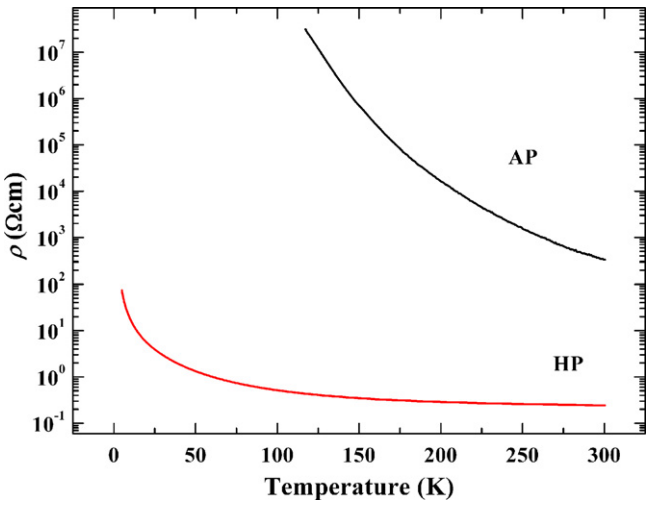

Fig. 3. Temperature dependences of electrical resistivity of the AP- and HP-$Ba_3CaIr_2O_9$.

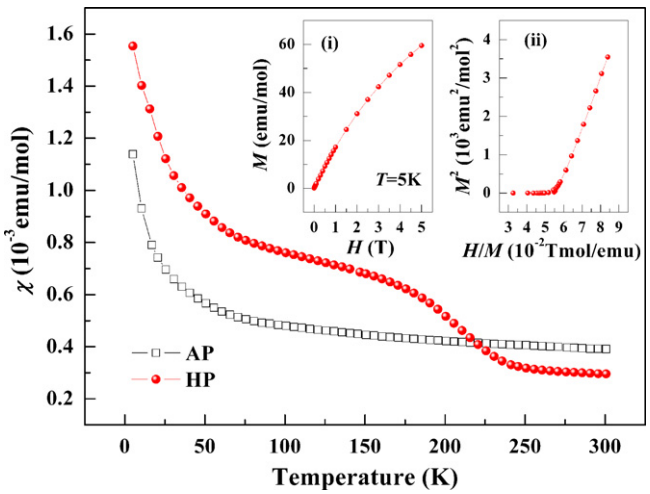

Fig. 4. Temperature dependences of magnetic susceptibility of the AP- and HP-$Ba_3CaIr_2O_9$. The inset (i) shows the magnetic field dependence of magnetization for the HP form at 5 K; (ii) shows the relationship of M^2 versus H/M converted from (i).

3.3. Magnetic properties

Fig. 4 shows the temperature dependences of magnetic susceptibility of the AP- and HP-$Ba_3CaIr_2O_9$. Since there is no obvious deviation between ZFC and FC curves, Fig. 4 only shows the ZFC modes. The inset (i) shows the magnetic field dependence of magnetization for the HP-$Ba_3CaIr_2O_9$ at 5 K, which indicates no long-range ferromagnetic order in the sample. The Arrott plot, i.e. M^2-(H/M) curve, is shown in the inset (ii), as converted from (i) [16]. The negative intercept on the M^2 axis, as obtained from the linear extrapolation of the high-field portion to $H = 0$, indicates that no spontaneous magnetization exits at 5 K. The magnetic susceptibility at low temperature is very small, with the value of 1.554×10^{-3} emu/mol at 5 K. For the HP-$Ba_3CaIr_2O_9$, there is a ferromagnetism-like transition at about 230 K in the χ–T curve. However, it is not ferromagnetic down to 5 K as indicated by the

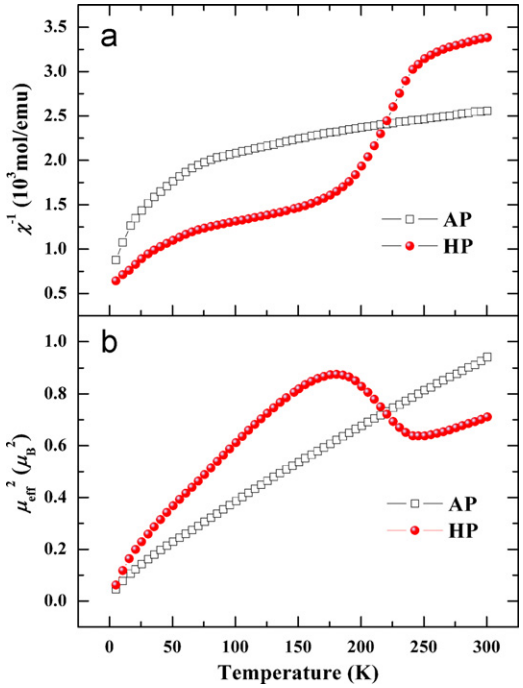

Fig. 5. Temperature dependences of (a) the inverse of magnetic susceptibility and (b) the square of μ_{eff} for the AP- and HP-$Ba_3CaIr_2O_9$.

M–H curve in the inset (i) of Fig. 4. This abnormal hoping is attributed to the exchange interaction between the two Ir cations in the adjacent IrO_6 octahedrons. The transition point is close to the Curie temperature T_c of Sr_2IrO_4 (250 K) [17] and $Sr_3Ir_2O_7$ (285 K) [12].

The relationships of reciprocal magnetic susceptibility versus temperature are not linear, as shown in Fig. 5(a). So their susceptibility does not follow the Curie law. Fig. 5(b) shows the temperature dependences of the square of the effective magnetic moment for the low spin configuration of Ir^{5+} ($\mu_{eff} = 3k_B\chi T/2N_A\mu_B^2$, where the k_B is the Boltzmann constant and N_A is Avogadro's number) for the AP- and HP-$Ba_3CaIr_2O_9$. The values of μ_{eff} are smaller than the theoretic value of about $2.83\mu_B$ calculated in the spin-only model for the two unpaired 5*d* electrons in the Ir^{5+} cations, which indicates that the Ir^{5+} cation loses partly local moment, which is attributed to the strong spin–orbit coupling. According to Kotani's theory [18], the relationship of $\mu_{eff}^2(Ir^{5+})$ versus temperature follows

$$\mu_{eff}^2(Ir^{5+}) \approx \frac{72k_BT}{\xi}, \quad (1)$$

where ξ is the spin–orbit coupling constant for Ir^{5+}. By fitting the $\mu_{eff}^2(Ir^{5+})$–*T* curves, we obtained the ξ of 15040(10) and 8760(14) cm^{-1} for the AP- and HP-$Ba_3CaIr_2O_9$, respectively. The fitting regions are 5–300 K and 5–150 K for the two forms, respectively. The values of ξ for the AP-$Ba_3CaIr_2O_9$ and HP-$Ba_3CaIr_2O_9$ indicate that the spin–orbit coupling is strong.

4. Conclusions

In summary, the high-pressure phase of $Ba_3CaIr_2O_9$ was synthesized using the high-pressure technique, and the XRD pattern, electrical resistivity, and magnetic susceptibility were obtained. Structural data indicated that it crystallizes into the 1:2 *B*-site-ordered perovskite. The measurements of electrical and magnetic properties showed that the HP-$Ba_3CaIr_2O_9$ is a paramagnetic semiconductor.

Acknowledgments

We thank Prof. C. Dong and H. Chen of Institute of Physics, Chinese Academy of Sciences for their help in XRD measurement and analysis, and the support from NSF and Ministry of Science and Technology of China through the research projects.

References

[1] T. Siegrist, B.L. Chamberland, J. Less-Common Met. 170 (1991) 93–99.
[2] R. Lindsay, W. Strange, B.L. Chamberland, R.O. Moyer Jr., Solid State Commun. 86 (1992) 759–763.
[3] J.G. Zhao, L.X. Yang, Y. Yu, F.Y. Li, R.C. Yu, C.Q. Jin, unpublished.
[4] S.-J. Kim, M.D. Smith, J. Darriet, H.-C. zur Loye, J. Solid State Chem. 177 (2004) 1493–1500.
[5] Y. Doi, Y. Hinatsu, J. Phys. Condens. Matter 16 (2004) 2849–2860.
[6] T. Sakamoto, Y. Doi, Y. Hinatsu, J. Solid State Chem. 179 (2006) 2595–2601.
[7] J.T. Rijssenbeek, T. Saito, S. Malo, M. Azuma, M. Takano, K.R. Poeppelmeier, J. Am. Chem. Soc. 127 (2005) 675–681.
[8] R.D. Shannon, Acta Crystallogr. A 32 (1976) 751–767.
[9] R.A. Young, The Rietveld Method, IUCr/OUP, Oxford, 1995.
[10] G. Cao, J.E. Crow, R.P. Guertin, P.F. Henning, C.C. Homes, M. Strongin, D.N. Basov, E. Lochner, Solid State Commun. 113 (2000) 657–662.
[11] G. Cao, J. Bolivar, S. McCall, J.E. Crow, R.P. Guertin, Phys. Rev. B 57 (1998) R11039–R11042.
[12] G. Cao, Y. Xin, C.S. Alexander, J.E. Crow, P. Schlottmann, M.K. Crawford, R.L. Harlow, W. Marshall, Phys. Rev. B 66 (2002) 214412 (1–7).
[13] P.D. Battle, J.B. Goodenough, R. Price, J. Solid State Chem. 46 (1983) 234–244.
[14] P.D. Battle, C.W. Jones, J. Solid State Chem. 78 (1989) 108–116.
[15] G. Demazeau, D.-Y. Jung, J.-P. Sanchez, E. Colineau, A. Blaise, L. Fournes, Solid State Commun. 85 (1993) 479–484.
[16] A. Arrott, Phys. Rev. 108 (1957) 1394–1396.
[17] M.K. Crawford, M.A. Subramanian, R.L. Harlow, J.A. Fernandez-Baca, Phys. Rev. B 49 (1994) 9198–9201.
[18] M. Kotani, J. Phys. Soc. Jpn. 4 (1949) 293–297.